



A computational, X-ray crystallographic and thermal stability analysis of TETROL and its pyridine and methylpyridine inclusion complexes



Benita Barton^{a,*}, Mino R. Caira^b, Eric C. Hosten^a, Cedric W. McClelland^a

^a Department of Chemistry, PO Box 77000, Nelson Mandela Metropolitan University, Port Elizabeth 6031, South Africa

^b Department of Chemistry, University of Cape Town, Rondebosch 7701, South Africa

ARTICLE INFO

Article history:

Received 22 May 2013

Received in revised form 15 July 2013

Accepted 30 July 2013

Available online 3 August 2013

Keywords:

Host–guest chemistry

Inclusion

TETROL

Methylpyridine

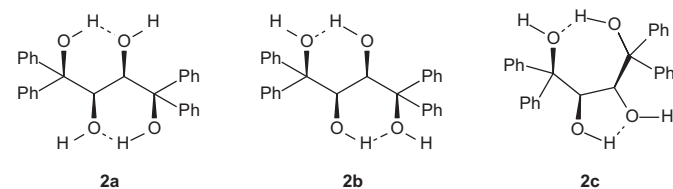
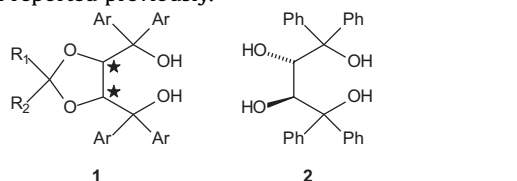
ABSTRACT

The identification and application of (+)-(2*R*,3*R*)-1,1,4,4-tetraphenylbutane-1,2,3,4-tetrol (TETROL) as an efficient and selective host compound is described. Computational and single crystal X-ray diffraction analyses revealed that the butane backbone of TETROL adopts a relatively rigid *anti*-conformation, with the hydroxy groups oriented *syn* and connected through a cyclic, homodromic arrangement of their O–H bonds. This structure is stabilised through a pair of 1,3-hydrogen bonding interactions. TETROL forms inclusion complexes with pyridine and 3- and 4-methylpyridine, and does so selectively from mixtures of the pyridines. X-ray diffraction (single crystal and powder) and thermal analyses of the inclusion compounds are described.

© 2013 Elsevier Ltd. All rights reserved.

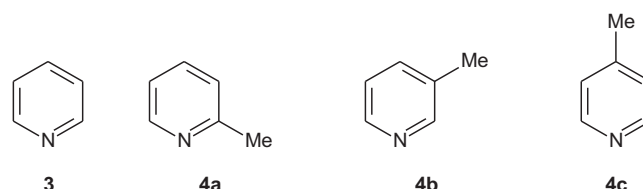
1. Introduction

The chiral auxiliaries TADDOLs ($\alpha,\alpha,\alpha,\alpha$ -tetraaryl-1,3-dioxolane-4,5-dimethanols) **1**, which are readily synthesised from inexpensive naturally-occurring tartaric acid, have been widely exploited as host compounds in inclusion complexes.^{1,2} We were intrigued by the possibility that the closely related compound, (+)-(2*R*,3*R*)-1,1,4,4-tetraphenylbutane-1,2,3,4-tetrol **2** (TETROL) might show similar potential. Although TETROL is not a novel compound,³ its use as an inclusion host compound has, to the best of our knowledge, not been reported previously.



Hydroxy groups are common structural features for both TETROL and the TADDOLs. An important feature of the TADDOL structure is rigidity, owing to the presence of the 1,3-dioxolane ring; structural rigidity is a property frequently associated with effective host compounds.⁴ However, in TETROL the conformational mobility usually associated with a butane chain could be significantly constrained as a result of intramolecular hydrogen bonding between the hydroxy groups. The expected favourable 1,3-interactions are shown in **2a** and **2b**; 1,2- and 1,4-interactions are also possible, as exemplified by **2c**. The resultant stiffening of the 1,2,3,4-tetrol moiety, coupled with its inter-molecular hydrogen bonding capability, would be expected to impart favourable inclusion host properties to TETROL.

This hypothesis was tested by performing a computational conformational analysis and an X-ray crystal structure determination on TETROL, and then by investigating host–guest interactions between TETROL and pyridine **3** as well as its methyl-substituted derivatives, 2-, 3- and 4-methylpyridine (**4a**, **4b** and **4c**, respectively).



* Corresponding author. Tel.: +27 41 504 4859; fax: +27 41 504 4236; e-mail addresses: benita.barton@nmmu.ac.za, benita.barton@gmail.com (B. Barton).

We now report on our findings.

2. Results and discussion

TETROL **2** was prepared from optically active (+)-diethyl L-tartrate using standard Grignard reaction methodology with phenyl magnesium bromide.

2.1. Conformational analyses

2.1.1. TETROL. A conformational search performed on TETROL at the molecular mechanics level using the MMFF force field[†] revealed the lowest energy conformers to comprise a family of structures with butane in the *anti* geometry, the four hydroxy groups in a *syn* arrangement on the butane backbone and stabilised through a pair of 1,3-hydrogen bonding interactions (Table 1 and Fig. 1). The hy-

This effect could increase the possibility of TETROL acting enantioselectively when forming complexes with other compounds.

In the next significantly less stable group of conformers (e.g., **2c**), the butane chain adopts a *gauche* conformation in which a 1,4-hydrogen bonding interaction is evident.

Although the ideal linear arrangement of the atoms involved in hydrogen bonding (O–H···O) is not achieved owing to the geometrical constraints of the intramolecular interaction, hydrogen bonding is nevertheless discernable from the directionality of the O–H bonds in the donor hydroxy groups, as well as the proximities of the interacting atoms. Inspection of the computed O–H···OH bond lengths (ranging from 1.62 Å to about 2.32 Å) indicates that the intramolecular hydrogen bonds range in strength from intermediate to weak (Table 1). The overall stabilisation achieved is significant, giving rise to barriers of about 98 kJ mol⁻¹ and 129 kJ mol⁻¹, respectively, to rotations about the C(1)–C(2) and C(2)–C(3) bonds of

Table 1
Computed energies and structural parameters[#] in conformers **2a–c** and **5a**

Computational level and conformers	Energy /kJ.mol ⁻¹	<i>E</i> _{rel} /kJ.mol ⁻¹	Intramolecular hydrogen bonding relationships and H···OH distances/Å									Torsion angle/°	
			1,2 (H1,O2)	1,3 (H1,O3)	1,2 (H2,O1)	1,2 (H2,O3)	1,3 (H2,O4)	1,3 (H3,O1)	1,2 (H3,O4)	1,4 (H4,O1)	1,3 (H4,O2)		1,2 (H4,O3)
MMFF													
2a	802.82	0		1.754	2.192				2.192		1.754		-178.3
2b	803.86	1.0	2.318				1.849	1.849					-171.4
2c	821.31	18.5				1.887					1.617		-66.3
5a	828.71	25.9				2.168			2.209	1.623			61.3
DFT (RB3LYP/6-31G*)													
2a	-3632392.49	1.0		1.853	2.068				2.068		1.853		176.5
2b	-3632393.53	0	2.146				1.863	1.863				2.146	179.5
2c	-3632364.35	29.2				1.858					1.728		-74.6
5a	-3632382.35	11.2		1.859							1.859		180.0
DFT (RB3LYP/6-31G*) aqueous [§]													
2a	-3632433.03	0		1.850	2.127				2.127		1.850		178.1
2b	-3632431.27	1.8	2.171				1.865	1.865				2.171	179.1
2c	-3632406.41	26.6									1.709		-75.6
5a	-3632426.89	6.1		1.824							1.824		180.0
DFT (RB3LYP/6-311G*)													
2a	-3633201.02	5.5		1.876	2.123				2.123		1.876		178.4
2b	-3633206.53	0	2.222				1.887	1.887				2.222	-179.9
5a	-3633198.54	7.9		1.870							1.870		180.0
DFT (RB3LYP/6-311++G**)													
2a	-3633415.54	4.5		1.878	2.183				2.183		1.878		179.0
2b	-3633420.01	0	2.279				1.916	1.916				2.279	-178.2
5a	-3633407.39	12.6		1.887							1.887		180.0

[#] The numbering sequence C(1)O(1)H(1)–C(2)O(2)H(2)–C(3)O(3)H(3)–C(4)O(4)H(4) was adopted for describing the relationships in Tables 1 and 2.

[§] The SM8 solvation model was used [A.V. Marenich, R.M. Olsen, C.P. Kelly, C.J. Cramer and D.G. Truhlar, *J. Chem. Theory Comput.*, **3**, 2011 (2007)].

The convention used in Spartan is for colors near red to represent large negative values of the electrostatic potential (electron-rich regions), while colors near blue represent large positive values (electron-poor regions); orange, yellow and green represent intermediate values.

droxy groups were found to adopt cyclic, homodromic arrangements of the O–H bonds in which a pair of weaker 1,2-hydrogen bonds possibly also contribute. The two lowest energy conformers **2a** and **2b** differ only in the clockwise and anti-clockwise orientations of the O–H bonds. In the case of **2a** the terminal hydroxy groups act as hydrogen bond donors[‡] and in **2b**, as hydrogen bond acceptors. Clearly, the chirality of the underlying C(2) and C(3) atoms influences the directionality of the hydrogen bonding array.

the butane unit in conformer **2a**.[§] The barriers arise from a combination of steric hindrance between bulky groups and disruption of the intramolecular hydrogen bonds.

The geometries of the three lowest energy structures were progressively refined further at the DFT level[¶], which confirmed the

[†] The MMFF force field has been explicitly parameterised to reproduce known hydrogen-bond distances.⁵

[‡] Understood in terms of the hydroxy group whose hydrogen atom becomes involved.

[§] The barriers were computed at the MMFF level by applying incremental rotations through 360° about the butane C(1)–C(2) and C(2)–C(3) bonds. Complex potential energy curves were obtained, characterised by several precipitous energy changes, which reflect the sudden release of pent-up strain energy as interfering groups rotate past each other, enabling the structure to snap into more stable conformations.

[¶] Geometry optimisations were performed with the B3LYP functional model successively employing the 6-31G*, 6-311G* and 6-311++G** basis sets.

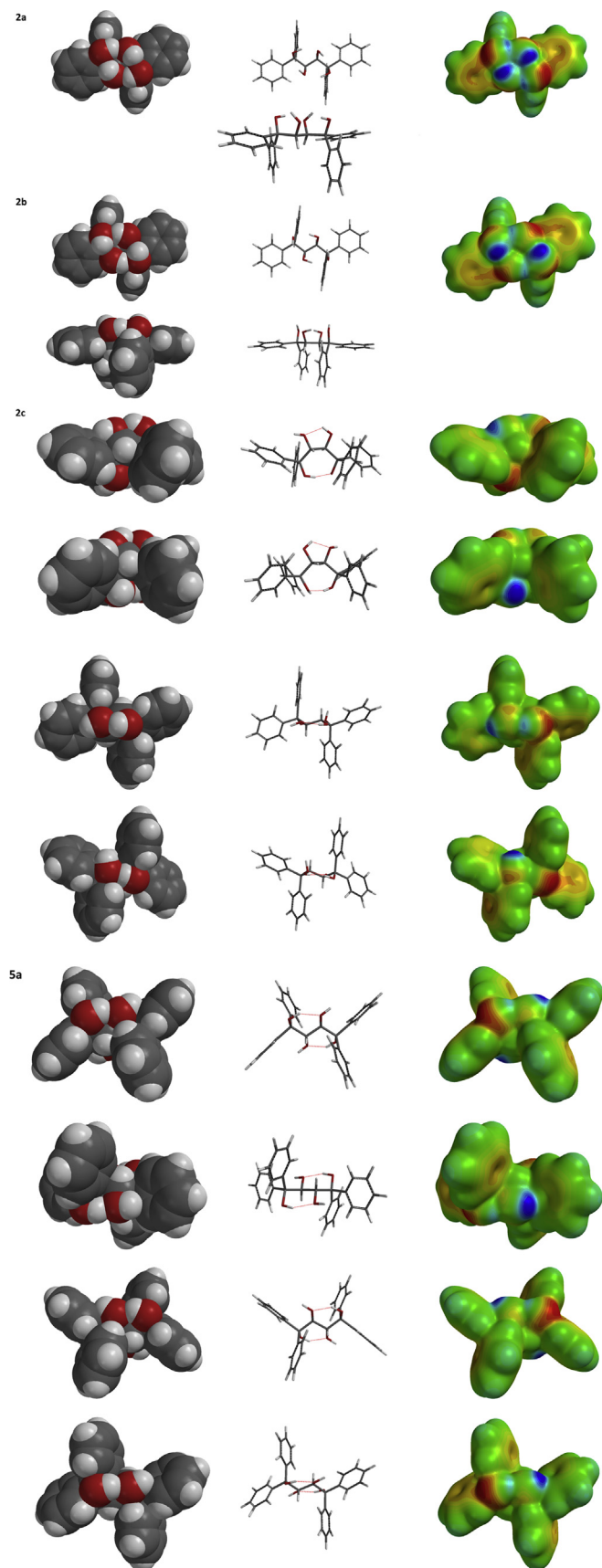


Fig. 1. Perspectives of the DFT optimised structures **2a–c** and **5a** and their electrostatic potential surfaces.

relative stability of the *anti* conformer. In vacuo calculations for all basis sets used reversed the stability order for conformers **2a** and **2b**, but the energy differences were small. Solvation effects were determined by repeating the B3LYP/6-31G* calculations using the SM8 aqueous solvation model; the stability order for **2a** and **2b** reverted to that found for the MMFF calculations, but again the energy difference was small (Table 1).

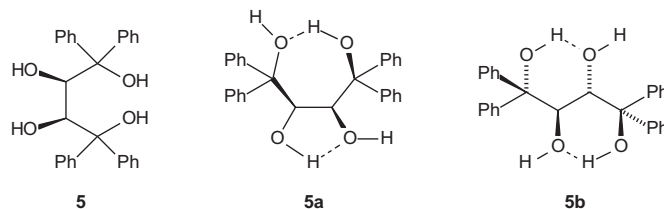
Inspection of the electrostatic potential surfaces computed for the optimised DFT structures (Fig. 1) is informative as they reveal the extents of the various hydrogen bonding interactions. For example, for structure **2b** the positive polarity associated with the hydrogen atoms of the C(2) and C(3) hydroxy groups is clearly dispersed as a result of their involvement in 1,3-hydrogen bonding. In contrast, the C(1) and C(2) hydroxy groups are more polar and consequently have potential for inter-molecular hydrogen bonding.

The computed conformers show some differences compared to the crystal structure of TETROL (vide infra) insofar as the four O–H bonds in the crystal adopt a linear rather than cyclic arrangement. The pair of intramolecular 1,3-hydrogen bonds is also evident in the crystal structure, while the C(2) and C(3) hydroxy groups are furthermore involved in inter-molecular hydrogen bonds (one as a donor and the other as an acceptor) with the corresponding hydroxy groups of a second TETROL molecule, which is located close by, with its array of hydroxy groups facing that of the first molecule (Fig. 2).

Single point energy calculations, followed by geometry optimisations, were carried out on this hydrogen bonded supramolecular motif (a TETROL dimer) at both the molecular mechanics and DFT levels. The geometry optimised structures were shown to be stabilised relative to TETROL at both computational levels, presumably as a result of the inter-molecular hydrogen bonding interactions (Table 2). The MMFF and DFT geometry optimisations both resulted in tighter intra- and inter-molecular hydrogen bonding interactions, compared to the crystal structure.

Changes in the relative orientations of the phenyl groups were also evident after the geometry optimisations. The MMFF optimisation minimised any steric interactions between adjacent rings, leaving both intramolecular pairs of ‘axial’ phenyl rings, as well as the two pairs of inter-molecular ‘equatorial’ phenyl rings, in face-on orientations (Fig. 2). In contrast, the twisted relative orientations of the phenyl rings in each of these pairs were largely retained in the DFT optimised structure, possibly reflecting the effect of CH– π interactions.

2.1.2. MESOTETROL. For comparison, the conformations of the corresponding *meso* isomer of TETROL, (2*R*,3*S*)-1,1,4,4-tetraphenyl butane-1,2,3,4-tetrol **5** (MESOTETROL) were also analysed. At the MMFF level, the lowest energy conformer was found to be the *gauche* conformation **5a**, which exhibits 1,4-hydrogen bonding and possibly also a weak 1,2-interaction. The nearest *anti* conformer, which displays a pair of 1,2-hydrogen bonds, was found to be about 4.6 kJ mol⁻¹ higher in energy. The next *anti* conformer, 7.7 kJ mol⁻¹ higher in energy than **5a**, is stabilised through a single 1,3-hydrogen bond as well as a weak 1,2 interaction. The first *anti* conformer, exhibiting a pair of 1,3-hydrogen bonds **5b**, was found to be 8.5 kJ mol⁻¹ higher in energy than **5a**.



Further refinement of the set of lower energy MMFF structures at the DFT level (B3LYP/6-31G*) gave **5b** as the most stable conformer, 18.5 kJ mol⁻¹ lower in energy than **5a**. In **5b** the two 1,3-

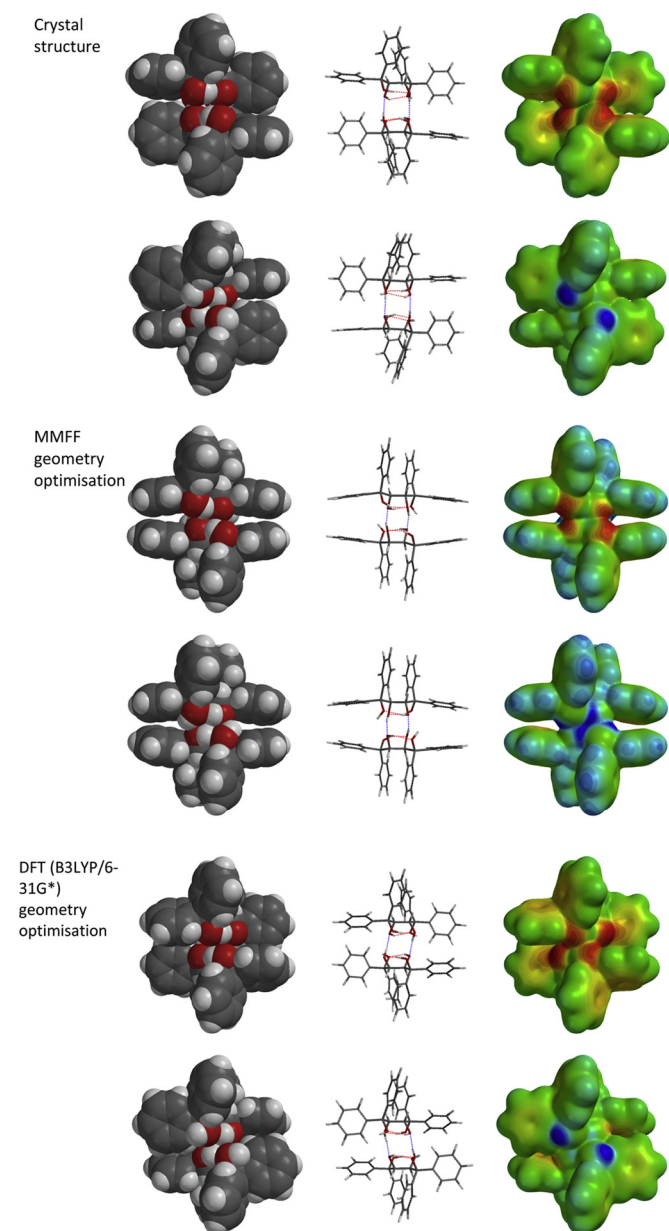


Fig. 2. Perspectives of the dimeric motif of TETROL and its electrostatic potential surface*. *The electrostatic potential energy surfaces of the crystal and MMFF structures were generated via single point DFT calculations on the respective molecular geometries.

dihydroxy units adopt an *anti* disposition on the butane chain, in contrast to *syn* in TETROL **2b**. The calculated dipole moment for **5b** is zero, in contrast to a value of 1.58 D for the lowest energy conformer of TETROL, **2b**. The lowest energy conformer found for MESOTETROL **5a** was 11.2 kJ mol⁻¹ less stable than its corresponding stereoisomer **2b** (Table 1).

The computed barrier to rotation about the C(2)–C(3) bond in **5** was about 89 kJ mol⁻¹, which is significantly lower than the corresponding value for **2**, implying that the *meso* isomer is likely to be a less rigid structure.

2.2. Single crystal X-ray crystallographic analysis of TETROL

Crystal data and refinement details are listed in Table 3 (Suitable crystals of TETROL were obtained by slow recrystallisation from ethanol). With six independent TETROL molecules in the crystal asymmetric unit, the volume of geometrical parameters for the TETROL molecular and crystal structure is extensive. Full lists of derived crystal and molecular parameters are provided as Supplementary data. A summary of the essential structural features follows.

Table 3
Crystallographic data for TETROL (**2**)

Chemical formula	C ₂₈ H ₂₆ O ₄
Formula weight	426.49
Crystal system	Trigonal
Space group	P3 ₁
μ (Mo K α)/mm ⁻¹	0.083
<i>a</i> /Å	23.7521(12)
<i>b</i> /Å	23.7521(12)
<i>c</i> /Å	20.5299(10)
α /°	90
β /°	90
γ /°	120
<i>V</i> /Å ³	10030.5(9)
<i>Z</i>	18
<i>F</i> (000)	4068
Temp	173(2)
Restraints	1
<i>N</i> _{ref}	16,611
<i>N</i> _{par}	1754
<i>R</i> 1	0.0313
<i>wR</i> 2	0.0771
<i>S</i>	1.004
θ min, max/°	1.71, 28.29
Tot. data	152,936
Unique data	16,611
Observed data [<i>I</i> > 2.0 σ (<i>I</i>)]	15,808
<i>R</i> _{int}	0.0511
Diffn measured fraction θ full	0.999
Min. resd. dens. (e/Å ³)	-0.213
Max. resd. dens. (e/Å ³)	0.264

Table 2
Computed energies and structural parameters for dimeric TETROL motif

Computational level and method	<i>E</i> /kJ.mol ⁻¹	<i>E</i> _{rel} /kJ.mol ⁻¹ *	Hydrogen bonding relationships and H...OH distances/Å						(C1,C2,C3,C4) torsion angle/°		Intersection angles for the planes of adjacent phenyl rings/°					
			Intramolecular				Intermolecular		A	B	<i>A</i> _{ax} / <i>A</i> _{ax}	<i>B</i> _{ax} / <i>B</i> _{ax}	<i>A</i> _{eq} / <i>B</i> _{eq}	<i>A</i> _{eq} / <i>B</i> _{eq}		
			A [§]		B [§]											
			[H1 _(A) ...O3 _(A)]	[H2 _(A) ...O4 _(A)]	[H1 _(B) ...O3 _(B)]	[H2 _(B) ...O4 _(B)]	[H3 _(A) ...O2 _(B)]	[H3 _(B) ...O2 _(A)]								
MMFF																
Single point	3829.41	2223.8	1.973	2.070	2.096	1.998	1.976	1.980	-169.7	-169.4	40.3	26.9	83.1	82.9		
Geometry optimisation	1576.79	-28.9	1.802	1.813	1.802	1.813	1.897	1.897	-166.9	-166.9	3.2	3.2	15.6	15.6		
DFT (B3LYP/6-31G*)																
Single point	-7262536.05	2251.0	1.973	2.070	2.096	1.998	1.976	1.980	-169.7	-169.4						
Geometry optimisation	-7264799.46	-12.4	1.819	1.889	1.816	1.890	1.832	1.835	-171.8	-171.8	15.9	15.9	70.2	71.8		

* The MMFF energies were calculated relative to twice the energy of **2a**, and the DFT energies relative to twice the energy of **5a**.

§ A and B refer to two TETROL molecules that make up the hydrogen-bonded pair.

The six crystallographically unique molecules (A–F) adopt similar conformations, the primary features being the common *anti*-conformation of the butane chain [the corresponding C–C–C–C dihedral angle spanning a narrow range from $-169.4(2)^\circ$ to $-172.2(2)^\circ$] while the four –OH groups are in a *syn* arrangement, displaying 1,3-H-bonding. A space-filling view of molecule A of TETROL as representative is shown in Fig. 3. It is noteworthy that in the crystal, the twofold symmetry of the homodromic hydrogen bonding motifs shown in 2a and 2b above is not manifested. Instead, only 1,3- and 2,4-hydrogen bonds stabilise the conformation while the –OH group at the 3-position is suitably disposed as a donor for inter-molecular hydrogen bonding to an oxygen atom

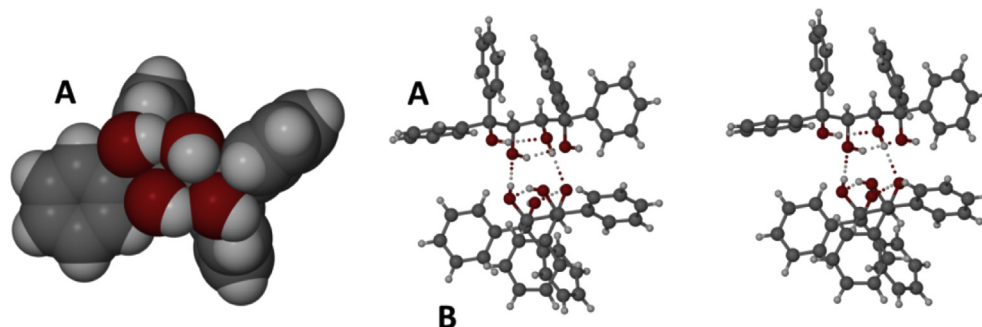


Fig. 3. Space-filling model of representative molecule A in the crystal of TETROL (left) and stereoview of a representative hydrogen bonded dimer (A–B) of TETROL (right).

acceptor at the 2-position of an adjacent molecule. The representative dimeric motif A–B shown in Fig. 3 is thus maintained by two inter-molecular O–H...O hydrogen bonds. Analogous interactions occur in dimers C–D and E–F.

Each of the three dimers is the repeating motif in an infinite column propagating parallel to the crystal *c*-axis via the threefold screw axis of the space group $P3_1$. A portion of this column is shown in Fig. 4 for the A–B pair as representative. This arrangement features two interwoven spiral chains of hydrogen bonds that maintain the columnar structure. All of the hydrogen bonding features reported for the six independent molecules of TETROL are based on the 24 hydroxyl group hydrogen atom positions that were observed in difference Fourier syntheses and subsequently idealised in a riding model with O–H=0.84 Å. Also shown in Fig. 4 is the complete crystal packing arrangement viewed along [001]. Geometrical data for the hydrogen bonds are included in the Supplementary data.

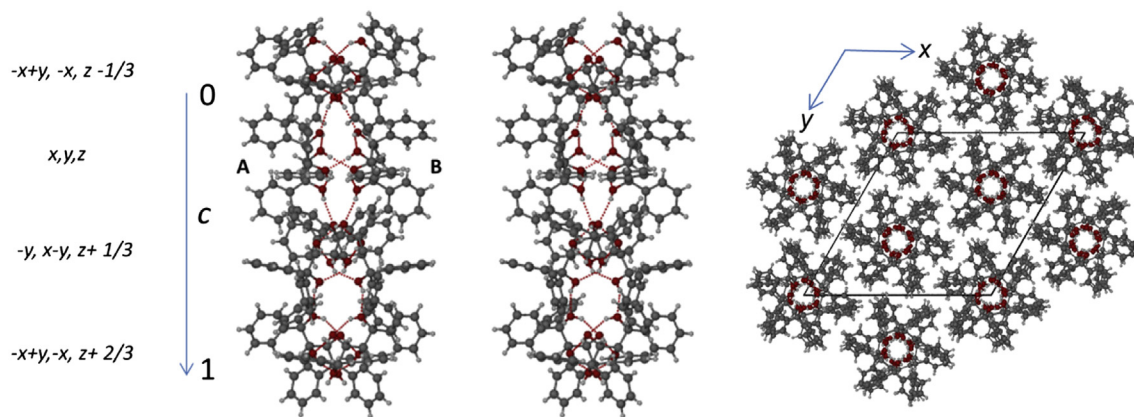


Fig. 4. Stereoview of a portion of a representative hydrogen bonded column comprising A–B dimers in TETROL (left) and crystal packing in TETROL viewed down the *c*-axis (right).

Given the somewhat unusual structural features of TETROL and its extensive hydrogen bonding capacity, its potential as a host compound was subsequently investigated.

2.3. Formation of inclusion complexes

TETROL 2 was dissolved separately in pyridine 3 and the methylpyridines 4a–c, and the solvents were then allowed to slowly evaporate under ambient conditions. The resulting crystals were collected, washed thoroughly with hexane and dried, all under suction filtration. ^1H NMR spectroscopy was used to determine the extent of inclusion and, where applicable, the host/guest (H/G) ratio (Table 4).

Of the four pyridines tested, only 2-methylpyridine 4a was not included by TETROL. The H/G ratio for the inclusion complex with pyridine was 1:2, while those of both 3- and 4-methylpyridine were 1:1.

Table 4
TETROL 2/guest (H/G) ratios of complexes formed

Guest (G)	H/G
Pyridine	1:2
2-Methylpyridine ^a	—
3-Methylpyridine	1:1
4-Methylpyridine	1:1

^a Crystallisation occurred with difficulty, requiring the addition of dichloromethane, methanol and hexane to the host and potential guest mixture.

2.4. Competition experiments

TETROL 2 was dissolved in equimolar mixtures of two or more pyridines and the solutions were then cooled to induce crystallisation. The resulting crystals were recovered, purified and analysed as described previously. H/G ratios of the resultant complexes are given in Table 5.

It is clear that TETROL is much more selective towards including 4-methylpyridine compared to the other pyridines (Table 5). This was the case for all solvent combinations involving 4-

Table 5
Competition experiments and H/G ratios of complexes formed

Pyridine	2-Methylpyridine	3-Methylpyridine	4-Methylpyridine	Guest ratios	Overall H/G ratio
		X	X	1:14	1:1
X	X		X	0:1	1:1
		X	X	1:4.5	1:1
X	X	X		1:3.7	1:1
X		X		1:1.7	1:1
X	X			0:0	1:0
	X	X	X	0:0:1	1:1
X	X	X	X	1:0:0:9	1:1

methylpyridine, including its binary mixtures with pyridine, 2-methylpyridine and 3-methylpyridine, respectively, as well as an equimolar ternary mixture containing 2-, 3- and 4-methylpyridine, and a quaternary mixture of pyridine and the three methylpyridines.

The competition experiments also showed that TETROL selects 3-methylpyridine over pyridine and 2-methylpyridine. It is interesting that in this case the 2-isomer was included from this mixture, albeit to a minor extent, even though no complex was obtained when TETROL was recrystallised from pure 2-methylpyridine. An experiment involving a mixture of pyridine and 2-methylpyridine showed no significant inclusion of either solvent. The presence of 2-methylpyridine appears to suppress the affinity of the host for pyridine.

With the exception of the last result, the overall H/G ratios were found to be 1:1 in the competition experiments, irrespective of the nature of the included guest.

The competition experiments show that the inclusion selectivity order displayed by TETROL is 4-methylpyridine > 3-methylpyridine > pyridine > 2-methylpyridine. Since the separation of mixtures of isomeric substituted pyridines, such as the methylpyridines through distillation is difficult owing to similar boiling points, their selective inclusion by TETROL could in principle be used to separate them. Heating the inclusion complex releases the guest (*vide infra*) and the host can then be recycled for further use. Pyridines are valuable building blocks in the synthesis of numerous agrochemicals, pharmaceuticals and polymers, amongst others,⁶ and hence the development of new methodologies for their purification is always interesting.

2.5. Thermal stability analyses

Differential scanning calorimetric (DSC) and thermogravimetric (TG) experiments were performed on the inclusion complexes of TETROL. Fig. 5a–f shows the thermal events that occurred when each complex was heated at a constant rate of 5 K min⁻¹ through the range 30–200 °C.

The mass losses observed for each of the complexes upon heating were close to their theoretically predicted values (Table 6). The guest compound release onset temperature for pyridine (43.8 °C) was the lowest of the three inclusion complexes, while the temperatures for the 3- and 4-methylpyridine complexes were similar (51.4 °C and 52.6 °C, respectively). The low initial release temperature for pyridine may be the reason for the slight discrepancy in overall weight loss for this complex (24.2% vs the predicted value of 27.1%) since some guest compound is probably lost during preparation of the sample for the thermal analyses.

The TG and DSC traces for the pyridine inclusion complex show that loss of pyridine occurs in three stages, with the last release at 105.3 °C (Fig. 5b). The thermal events evident for the inclusion complexes of TETROL with 3- and 4-methylpyridine are simpler than for pyridine (Fig. 5c–f). They are themselves similar, the main difference being the shift to a higher temperature of the endotherm

associated with the ultimate release of 3-methylpyridine (115.4 °C, peak maximum), compared to 4-methylpyridine (130.8 °C).

In all three cases there is a small endotherm between 142 and 143 °C, just prior to the host melting, and is possibly due to a phase change in the host.

The term ($T_{\text{on}} - T_{\text{b}}$), where T_{on} is the onset temperature of guest release and T_{b} the boiling point of pure guest, has long been used as an indicator of the relative stabilities of complexes.⁷ The more positive this value is found to be for a particular host, the more stable the complex is considered. In the present case the values for ($T_{\text{on}} - T_{\text{b}}$) are negative for all three complexes (Table 6), and their suggested stability is in the order pyridine > 4-methylpyridine ≈ 3-methylpyridine. This contradicts the host selectivity order that emerged from competition experiments where the inclusion of 4-methylpyridine was favoured over the other pyridines. The lack of crystal isostructurality among the three complexes is possibly a factor, which renders the predictive value of the parameter ($T_{\text{on}} - T_{\text{b}}$) less reliable. In the present case, the peak temperatures at which the last of the guest compounds are released (T_{pr}) correlate best with the inclusion selectivities arising from the competition experiments (Table 6).

2.6. Powder diffraction patterns

The polymorphic characteristics of the host residue after release of the guest were determined by obtaining the X-ray powder diffraction patterns for the residues in all three cases (Supplementary data). Identical powder diffraction patterns were found, indicating that the same polymorph had been obtained in each of the three cases. The patterns were furthermore similar to that obtained for the host compound prior to complexation, but matched the pattern computed from the single crystal X-ray analysis very well. From the latter, we deduce that the initial sample of TETROL was affected to some extent by preferred orientation.

2.7. Single crystal X-ray diffraction analyses of the 2·pyridine, 2·3-methylpyridine and 2·4-methylpyridine inclusion complexes

The X-ray crystallographic data (Table 7) show that the three complexes belong to different crystal systems, namely, triclinic for the 2·pyridine complex (space group $P1$), orthorhombic for the 2·3-methylpyridine complex ($P2_12_12_1$) and monoclinic for the 2·4-methylpyridine complex ($C2$). Figs. 6–8 show the unit cells for the three complexes, with the guest in space-filling representation. Hydrogen bonds are highlighted with light blue dashed lines. Disorder across a centre of inversion was noted for the guest in the case of 2·4-methylpyridine, the two components being present with site-occupancies 0.5 each (Fig. 8). In both the pyridine and 4-methylpyridine complexes (where the guest molecules are symmetrical structures), the angles subtended by the intersecting planes of the geminal phenyl rings in each CPh₂OH group are either very similar [105.1(11)° and 105.9(13)° for the pyridine complex or identical [108.7(13)° for the 4-methylpyridine complex]. The intersection angles differ significantly when 3-methylpyridine is the included guest, with values of 95.2(8)° and 109.8(8)° being observed. The unsymmetrical alignment of the geminal pairs of phenyl rings is most likely due to the unsymmetrical guest molecule in this case. The pyridine guest molecules are found in continuous, though somewhat constricted, channels (Fig. 9), while both the 3- and 4-methylpyridine guest molecules occupy discrete cavities in the host frameworks (Figs. 7 and 8).

It has been noted that for a specific host compound, the inclusion complexes in which the guest molecules reside in channels, generally have lower relative thermal stabilities than those in which the guests are contained in isolated cavities in the host

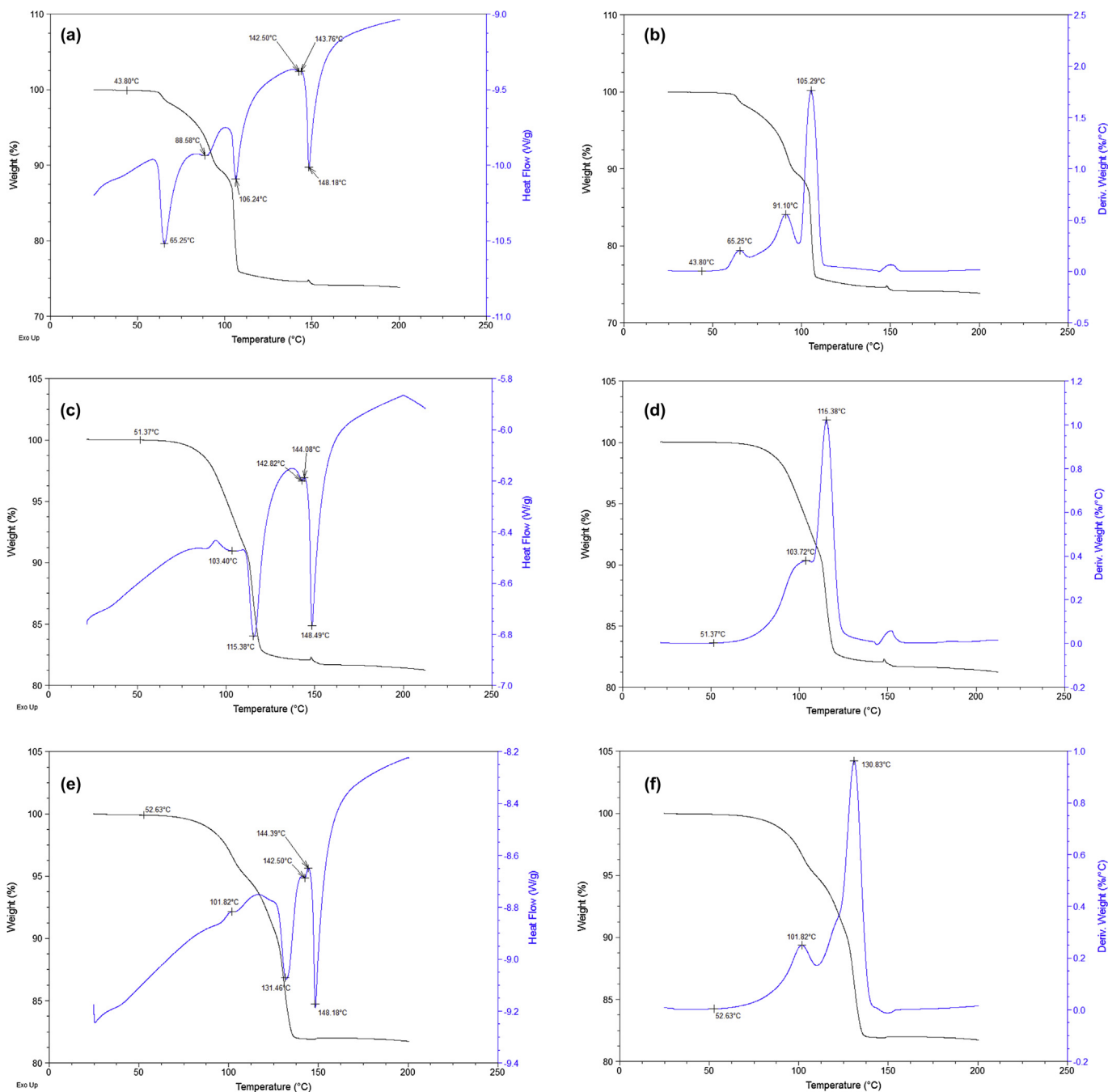


Fig. 5. (a) DSC and TG traces (overlaid) for 2-pyridine; (b) TG and its derivative for the 2-pyridine complex (c) DSC and TG traces (overlaid) for 2-3-methylpyridine; (d) TG and its derivative for the 2-3-methylpyridine complex (e) DSC and TG traces (overlaid) for 2-4-methylpyridine; (f) TG and its derivative for the 2-4-methylpyridine complex.

Table 6

Thermal data from DSC/TG traces for 2-pyridine, 2-3-methylpyridine and 2-4-methylpyridine

Guest	$T_{on}/^{\circ}C^a$	$T_b/^{\circ}C$	$(T_{on}-T_b)/^{\circ}C$	$T_{pf}^{a,b}$	Observed mass loss (%)	Expected mass loss (%)
Pyridine	43.8	115	-71.2	105.3	24.2	27.1
3-Methylpyridine	51.4	144	-92.6	115.4	17.3	17.9
4-Methylpyridine	52.6	145	-92.4	130.8	17.8	17.9

^a Estimated from the TG derivatives (Figs. 4, 6 and 8).

^b The peak temperature at which the last of the guest is released.

crystal.⁸ In the latter case, complete disruption of the host framework, necessitating a higher temperature, is required to release the guests, while channel-occupying guests are able to diffuse out at lower temperatures. Our findings from the thermal stability studies showed that the pyridine complex is less stable than the two

methylpyridine complexes. This can be attributed to the fact that the pyridine molecules occupy channels rather than discrete cavities.

Figs. 10–12 are stereoviews of the guest packing arrangements in the crystals. Only 1,3-intramolecular and no inter-molecular

Table 7
Crystallographic data for 2·pyridine, 2·3-methylpyridine, 2·4-methylpyridine

	2·Pyridine	2·3-Methylpyridine	2·4-Methylpyridine
Chemical formula	C ₂₈ H ₂₆ O ₄ ·2C ₅ H ₅ N	C ₂₈ H ₂₆ O ₄ ·C ₆ H ₇ N	C ₂₈ H ₂₆ O ₄ ·C ₆ H ₇ N
Formula weight	584.69	519.61	519.61
Crystal system	Triclinic	Orthorhombic	Monoclinic
Space group	P1	P2 ₁ 2 ₁ 2 ₁	C2
μ (Mo K α)/mm ⁻¹	0.083	0.081	0.080
a/Å	8.2430(2)	10.5753(4)	17.8433(8)
b/Å	9.7660(2)	14.6758(5)	8.1284(4)
c/Å	10.8739(9)	17.8006(6)	12.7853(6)
α /°	90.663	90	90
β /°	108.101(1)	90	131.175(1)
γ /°	113.368	90	90
V/Å ³	754.62(3)	2762.67(17)	1395.77(12)
Z	1	4	2
F(000)	310	1104	552
Temp	150	150	200
Restraints	3	0	1
Nref	3732	3835	1830
Npar	405	361	213
R	0.0336	0.0310	0.0330
wR2	0.0908	0.0881	0.0898
S	1.04	1.03	1.05
θ min–max/°	2.3, 28.4	2.2, 28.3	2.3, 28.3
Tot. data	38,700	29,517	15,317
Unique data	3732	3835	1830
Observed data [I > 2.0 σ (I)]	3666	3627	1780
R _{int}	0.016	0.017	0.016
Dffrn measured fraction θ full	0.992	0.998	0.994
Min. resd. dens. (e/Å ³)	–0.26	–0.16	–0.17
Max. resd. dens. (e/Å ³)	0.29	0.28	0.27

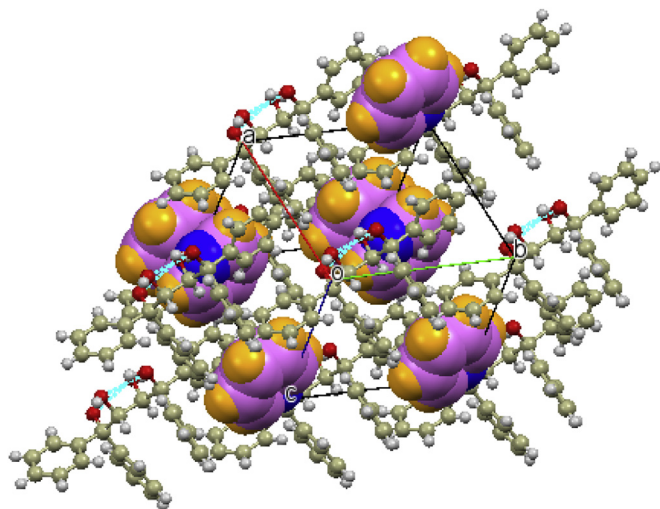


Fig. 6. Unit cell for the 1:2 complex of **2** with pyridine; the guest is shown in space-filling representation and hydrogen bonding by means of dashed light blue lines.

O–H···OH hydrogen-bonding is observed in the pyridine complex. The host framework is thus expected to be less rigid, possibly allowing for more facile guest escape. The pyridine molecules themselves are held in the crystal by means of (guest) N···H–O(host) hydrogen bonds (N···O 2.742(2) and 2.754(2) Å). The complex is further stabilised by guest–guest as well as host–guest aromatic ring π – π stacking interactions. Only weak CH– π interactions were observed between the host and guest [(guest)*meta*-C–H···Ar(host) and (host)*meta*-C–H···Ar(guest)], ranging from 3.55 to 3.8 Å (133–151°).

Reasons for the lower thermal stability of the 3-methylpyridine complex relative to that of the 4-methylpyridine analogue are

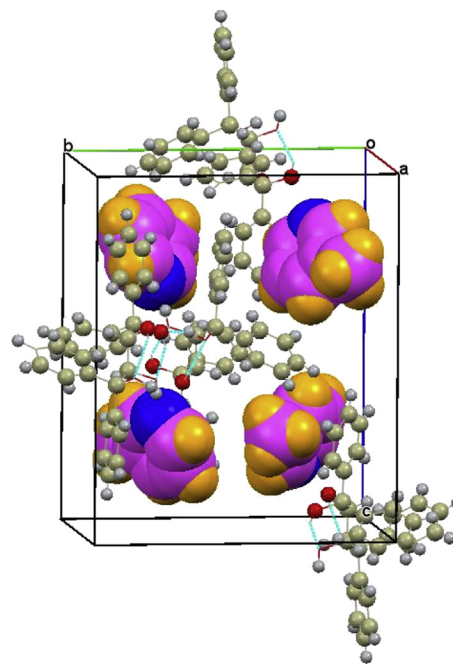


Fig. 7. Unit cell for the 1:1 complex of **2** with 3-methylpyridine.

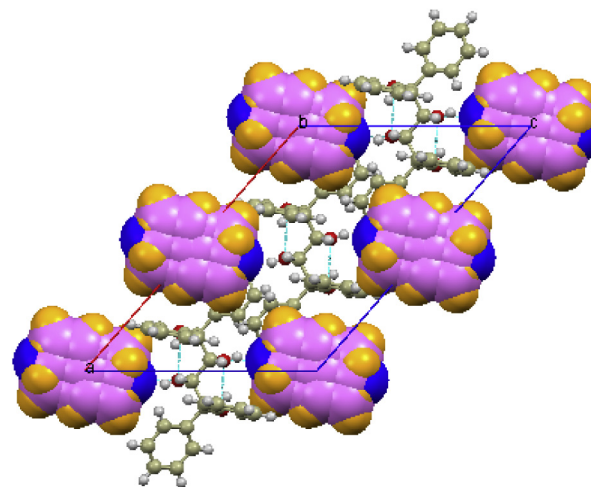


Fig. 8. Unit cell for the 1:1 complex of **2** with 4-methylpyridine.

less clear. Both guests engage in (guest)N···H–O(host) hydrogen bonds that of 3-methylpyridine being marginally stronger [2.7094(18) Å] compared with the 4-methyl isomer [2.790(5) Å]. No intramolecular π – π stacking interactions are observed in either complex. Furthermore, no inter-molecular host···host hydrogen bonds occur in the 4-methylpyridine complex, though they are apparent in the 3-methylpyridine complex [CPh₂OH···O(H)CPh₂ (2.7233(15) Å) and *ortho* Ar–CH···O(H)CH (3.2603(18) Å)]. However, weak π – π interactions, which are evident between the host and the 4-methylpyridine guest molecules [4.139(2) Å] are not significant in the 3-methylpyridine case, which may account for the observed thermal stability difference. A contributing factor may be that each guest molecule in the 4-methylpyridine complex experiences two weak CH– π interactions with a host aromatic ring: the C3 and C5 hydrogens of 4-methylpyridine interact favourably with host aromatic rings [3.658(7) Å and 3.670(6) Å, with angles of 148° and 147°, respectively], while only one guest CH₂H···host aromatic CH– π interaction is observed per guest molecule in the 3-methylpyridine case [3.635(2) Å, 166°].

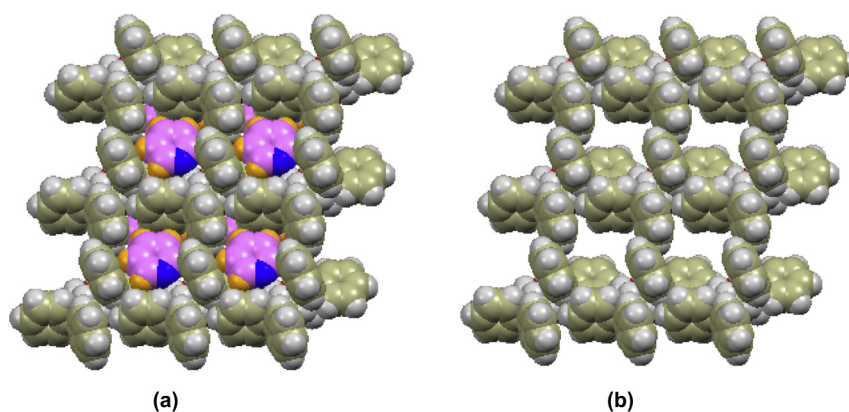


Fig. 9. (a) The 1:2 complex of **2** with pyridine showing the channel-occupation of the guest; the view is along the *a*-axis, and the structure shown is several molecules thick; (b) the guest has now been deleted to show the channels more clearly.

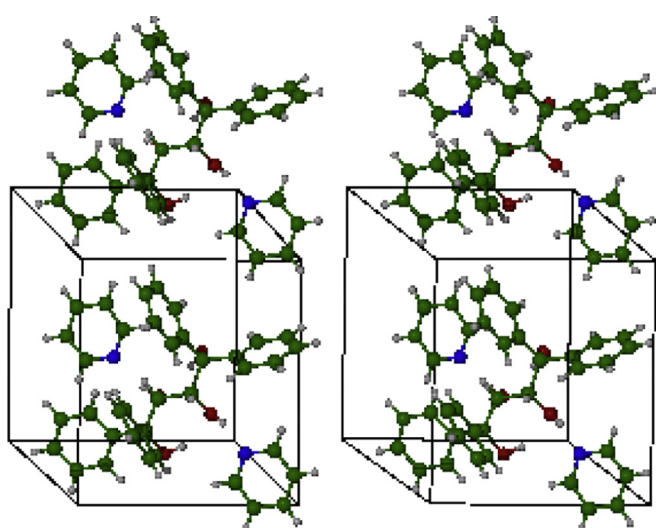


Fig. 10. Stereoview of the 1:2 complex of **2** with pyridine.

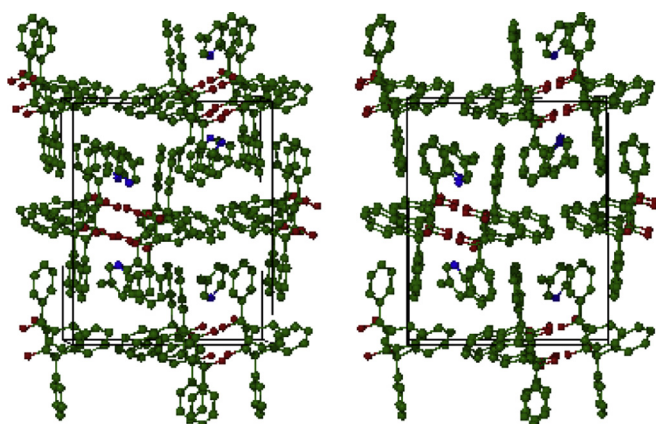


Fig. 11. Stereoview of the 1:1 complex of **2** with 3-methylpyridine (hydrogens omitted for clarity).

3. Conclusions

A computational conformational analysis of TETROL at both the molecular mechanics and DFT levels revealed that in the lowest energy structure the conformation of the butane chain is *anti*, with the four hydroxy groups in a *syn* arrangement with respect to the butane backbone, and involved in a pair of 1,3-hydrogen bonding

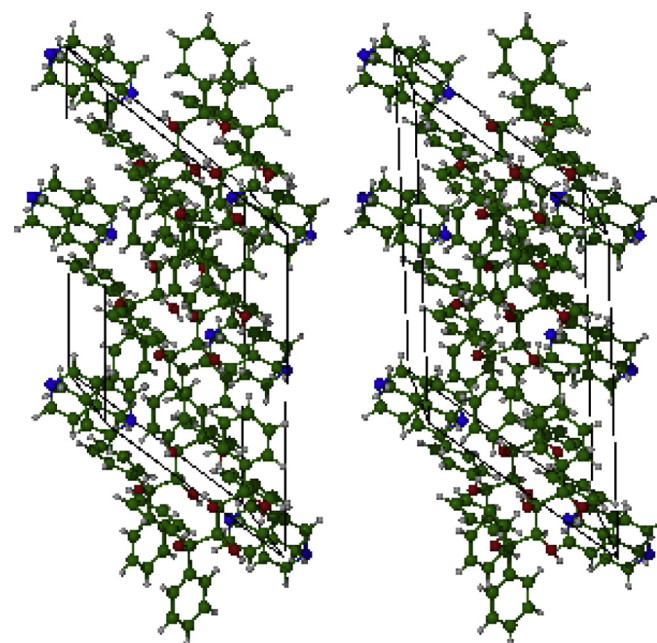


Fig. 12. Stereoview of the 1:1 complex of **2** with 4-methylpyridine.

interactions. The stabilisation achieved through intramolecular hydrogen bonding is significant, giving rise to a calculated (MMFF) barrier of about 129 kJ mol^{-1} to rotation about the C(2)–C(3) bond of the butane unit. The resultant rigidity of the butane backbone was predicted to impart favourable host characteristics to TETROL when involved in inclusion complexation. This was confirmed by the formation of inclusion complexes when the host was recrystallised from pyridine and 3- and 4-methylpyridine. The pyridines were included selectively when TETROL was recrystallised from binary, ternary and quaternary mixtures of the pyridines, with the preference order being 4-methylpyridine > 3-methylpyridine > pyridine > 2-methylpyridine. Thermal stability studies were carried out on the three inclusion complexes. The X-ray crystal structures of TETROL and its inclusion complexes were determined, with the insights obtained into the inter-molecular interactions allowing the thermal stabilities of the complexes to be rationalised. It is proposed that the inclusion selectivity displayed by TETROL could be used for separating the isomeric methylpyridines.

The obvious potential of TETROL as a host compound is currently being explored in our laboratories. It forms complexes with numerous guest species, and enantiomeric separations have been

achieved when TETROL was recrystallised from racemates, due to the chiral environment it provides to chiral guest species. Further communications in this regard are imminent.

4. Experimental

4.1. General

Melting points were recorded on an Electrothermal IA9000 Series digital melting point apparatus and are uncorrected. Infrared spectra were recorded on a Bruker Tensor 27 Platinum ATR system and analysed using Opus version software. ^1H and ^{13}C NMR spectra were obtained using a Bruker Ultrashield Plus 400 MHz spectrometer and analysed using TopSpin 3.0 software. DSC and TG traces were collected using a TA SDT Q600 Module system and analysed using TA Universal Analysis 2000 data analysis software. Samples were placed in open ceramic pans with an empty ceramic pan functioning as a reference. High purity nitrogen gas was used as purge gas. Optical rotations were measured using an A. Krüss Optronic polarimeter (Germany) equipped with a sodium lamp.

4.2. Computational studies

Calculations were performed using SPARTAN '10 for Windows [build 1.1.0 (Mar 20 2011)] software, supplied by Wavefunction Inc. Conformational searches were carried out using the Monte Carlo algorithm as implemented in the MMFF (Merck Pharmaceuticals) force field; the first one hundred lowest energy conformations were retained. Only structures whose relative energies fell within the first 20 kJ mol^{-1} range were refined further at the DFT level using the B3LYP functional and progressively employing the 6-31G*, 6-311G*, and 6-311++G** basis sets. The SCF procedure used restricted hybrid HF-DFT calculations with Pulay DIIS and geometric direct minimisation. Solvation effects were determined by repeating the B3LYP/6-31G* calculations using the SM8 aqueous solvation model.

4.3. Synthesis of (+)-(2R,3R)-1,1,4,4-tetraphenylbutane-1,2,3,4-tetrol 2

This compound was synthesised according to a standard Grignard procedure using excess PhMgBr . Addition of the tartrate to the Grignard reaction was highly exothermic and thus this step was carried out with cooling in an ice-water bath. In a typical reaction, the use of bromobenzene (22.99 g, 146.5 mmol) and magnesium turnings (3.94 g, 162.0 mmol) in anhydrous THF, with (+)-diethyl L-tartrate (5.00 g, 24.3 mmol), also in anhydrous THF, afforded a gum, which was crystallised and recrystallised from CH_2Cl_2 /hexane/MeOH to afford (+)-(2R,3R)-1,1,4,4-tetraphenylbutane-1,2,3,4-tetrol 2 as a white solid (4.68 g, 10.9 mmol, 45%), mp 147–149 °C (lit.,³ mp 150–151 °C); $[\alpha]_{\text{D}}^{23} +166$ (c 9.32, CH_2Cl_2) {lit.,³ $[\alpha]_{\text{D}}^{25} +154$ (c 1.2, CHCl_3)}; $\nu_{\text{max}}(\text{solid})/\text{cm}^{-1}$ 3440 (br, OH), 3294 (br, OH), 3057 (Ar), 3033 (Ar), 1598 (Ar) and 1494 (Ar); δ_{H} (CDCl_3) 3.86 (2H, d, 2COH), 4.44 (2H, d, 2HCOH), 4.72 (2H, s, 2CPh₂OH) and 7.2–7.4 (20H, m, Ar); δ_{C} (CDCl_3) 72.11 (HCOH), 81.71 (CPh₂OH), 124.97 (Ar), 126.05 (Ar), 127.15 (Ar), 127.27 (Ar), 128.10 (Ar), 128.37 (Ar), 128.55 (Ar), 130.08 (Ar), 143.85 (quaternary Ar) and 144.16 (quaternary Ar).

4.4. Powder diffraction patterns

These were obtained by subjecting the powders to Cu $K\alpha_1$ radiation ($\lambda=1.54056$ Å) using a Bruker D2 diffractometer. The scan range was from 5 to 50° at 0.01 steps/s. A Ni filter was used at the Lynxeye detector. Samples were prepared by heating the inclusion complexes to expel the guest compounds, and

discontinuing heating just before the melting point of the host was reached.

4.5. Single crystal X-ray diffraction

X-ray diffraction studies of the three inclusion complexes were performed at 150 K or 200 K using a Bruker Kappa Apex II diffractometer with graphite-monochromated Mo $K\alpha$ radiation ($\lambda=0.71073$ Å). APEXII⁹ was used for data collection and SAINT⁹ for cell refinement and data reduction. The structure was solved by direct methods using SHELXS-97¹⁰ and refined by least-squares procedures using SHELXL-97¹⁰ with SHELXLE¹¹ as a graphical interface. All non-hydrogen atoms were refined anisotropically. C-bound H atoms were placed in calculated positions and refined as riding atoms, with C–H 1.00 (CH), 0.95 (aromatic CH), 0.98(CH₃) Å and with $U(\text{H})=1.2(1.5$ for methyl) $U_{\text{eq}}(\text{C})$. The H atoms of the methyl groups were allowed to rotate with a fixed angle around the C–C bond to best fit the experimental electron density (HFIX 137 in the SHELX program suite¹⁰). The H atoms of the hydroxy groups were allowed to rotate with a fixed angle around the C–O bond to best fit the experimental electron density (HFIX 148 in the SHELX program suite¹⁰) with $U(\text{H})$ set to 1.5 $U_{\text{eq}}(\text{O})$. Data were corrected for absorption effects using the multi-scan method implemented in SADABS.⁹ In the absence of significant anomalous scattering, Friedel pairs were merged and the absolute structure was assigned by reference to an unchanging chiral centre in the synthetic procedure.

The crystals of TETROL required special treatment as they were found to be merohedral twins. Structure solution involved location of six independent molecules of TETROL and was achieved using SHELXD.¹⁰ However, the model failed to refine below $R1=0.22$. The twofold nature of the twinning was revealed by PLATON¹² and subsequent corrections led to rapid convergence of the refinement of the non-H atoms, first isotropically and then anisotropically (SHELXL-97¹⁰ operating under the X-Seed graphical interface¹³). Successful treatment of the data led to the location of all H atoms (including those of the 24 independent hydroxyl groups) in successive difference Fourier syntheses. They were included in idealised positions as described for the complexes above with U values 1.2 times those of their parent atoms. Refinement converged with a BASF parameter of 0.444(1) for the crystal specimen studied. Since the absolute configuration was known from the synthesis, and the Flack parameter did not discriminate enantiomers, the Bijvoet pairs were merged (MERG 4 in SHELXL-97¹⁰).

Acknowledgements

Financial support is acknowledged from the Nelson Mandela Metropolitan University, and E. Ferg is thanked for performing powder diffraction analyses. M.R.C. thanks the University of Cape Town and the National Research Foundation (Pretoria) for financial support.

Supplementary data

CCDC-915557, 915561, 915570 and 924355 contain the supplementary crystallographic data for this paper. These data can be obtained free of charge from The Cambridge Crystallographic Data Centre via www.ccdc.cam.ac.uk/data_request/cif. Full geometrical data for the structure of TETROL and PXRD traces are included in the Supplementary Data. Supplementary data related to this article can be found at <http://dx.doi.org/10.1016/j.tet.2013.07.094>.

References and notes

1. Seebach, D.; Beck, A. K.; Heckel, A. *Angew. Chem., Int. Ed.* **2001**, *40*, 92.
2. Caira, M. R.; Tanaka, K. *Top. Heterocycl. Chem.* **2009**, *18*, 75.
3. Shan, Z.; Hu, X.; Zhou, Y.; Peng, X.; Li, Z. *Helv. Chim. Acta* **2010**, *93*, 497.
4. Weber, E.; Skobridis, K.; Wierig, A.; Nassimbeni, L. R.; Johnson, L. J. *Chem. Soc., Perkin Trans. 2* **1992**, 2123.
5. Hehre, W. H. *A Guide to Molecular Mechanics and Quantum Mechanical Calculations*; Wavefunction: Irvine, USA, 2003; p 176.
6. Sagitullin, R. S.; Shkil, G. P.; Nosonova, I. I.; Ferber, A. A. *Chem. Heterocycl. Compd.* **1996**, *32*, 127.
7. (a) Caira, M. R.; Nassimbeni, L. R.; Niven, M. L.; Schubert, W.-D.; Weber, E.; Dörpinghaus, N. *J. Chem. Soc., Perkin Trans. 2* **1990**, 2129; (b) Bourne, S. A.; Nassimbeni, L. R.; Weber, E.; Skobridis, K. *J. Org. Chem.* **1992**, *57*, 2438; (c) Barbour, L. J.; Caira, M. R.; Nassimbeni, L. R. *J. Chem. Soc., Perkin Trans. 2* **1993**, 1413.
8. Tanaka, K.; Hori, K.; Tsuyuhara, S.; Motoki, S.; Shide, S.; Arakawa, R.; Caira, M. R. *Tetrahedron* **2013**, *69*, 1120.
9. APEX2, SADABS and SAINT; Bruker AXS: Madison, Wisconsin, USA, 2010.
10. Sheldrick, G. M. *Acta Crystallogr.* **2008**, *A64*, 112.
11. Hübschle, C. B.; Sheldrick, G. M.; Dittrich, B. *J. Appl. Crystallogr.* **2011**, *44*, 1281.
12. Spek, A. L. *J. Appl. Crystallogr.* **2003**, *36*, 7.
13. Barbour, L. J. *Supramol. Chem.* **2001**, *1*, 189.